ELSEVIER

Contents lists available at ScienceDirect

Quaternary Science Reviews

journal homepage: www.elsevier.com/locate/quascirev





Timing of Cordilleran-Laurentide ice-sheet separation: Implications for sea-level rise

Alberto V. Reyes ^{a,**}, Anders E. Carlson ^b, Jorie Clark ^c, Louise Guillaume ^d, Glenn A. Milne ^e, Lev Tarasov ^f, Elizabeth C.B. Carlson ^g, Feng He ^h, Marc W. Caffee ⁱ, Klaus M. Wilcken ^j, Dylan H. Rood ^{d,*}

- ^a Department of Earth and Atmospheric Sciences, University of Alberta, Edmonton, AB T6G 2E3, Canada
- b Oregon Glaciers Institute, Corvallis, OR 97330, USA
- ^c College of Earth, Ocean, and Atmospheric Sciences, Oregon State University, Corvallis, OR 97331, USA
- ^d Department of Earth Science and Engineering, Royal School of Mines, Imperial College London, SW7 2AZ, UK
- ^e Department of Earth Sciences, University of Ottawa, Ottawa, ON K1N 6N5, Canada
- f Department of Physics and Physical Oceanography, Memorial University, St. John's, NL A1C 5S7, Canada
- g Burpee Museum of Natural History, Rockford, IL 61103, USA
- h Center for Climatic Research, Nelson Institute for Environmental Studies, University of Wisconsin-Madison, Madison, WI 53706, USA
- i Department of Astronomy and Physics & Department of Earth, Atmospheric, and Planetary Sciences, Purdue University, West Lafayette, IN 47907, USA
- ^j Australian Nuclear Science and Technology Organization, New Illawarra Road, Lucas Heights, NSW, 2234, Australia

ARTICLE INFO

Handling Editor: Dr C. O'Cofaigh

Keywords:
Pleistocene
Glaciation
North America
Cosmogenic isotopes
Laurentide ice sheet
Cordilleran ice sheet
Sea-level rise
Meltwater pulse 1A
Saddle collapse

ABSTRACT

During the last deglaciation, collapse of the saddle between the North American Cordilleran and Laurentide ice sheets led to rapid ice-sheet mass loss and separation, with meltwater discharge contributing to deglacial sealevel rise. We directly date ice-sheet separation at the end of the saddle collapse using 64 ^{10}Be exposure ages along an $\sim\!1200\text{-km}$ transect of the ice-sheet suture zone. Collapse began in the south by 15.4 ± 0.4 ka and ended by 13.8 ± 0.1 ka at $\sim\!56^\circ\text{N}$. Ice-sheet model simulations consistent with the ^{10}Be ages find that the saddle collapse contributed 6.2–7.2 m to global mean sea-level rise from $\sim\!15.5$ ka to $\sim\!14.0$ ka, or approximately one third of global mean sea-level rise over this period. We determine 3.1–3.6 m of the saddle collapse meltwater was released during Meltwater Pulse 1A $\sim\!14.6$ -14.3 ka, constituting 20–40% of this meltwater pulse's volume. Because the separation of the Cordilleran and Laurentide ice sheets occurred over 1–2 millennia, the associated release of meltwater during the saddle collapse supplied a smaller contribution to the magnitude of Meltwater Pulse 1A than has been recently proposed.

1. Introduction

During the Last Glacial Maximum (LGM), the Cordilleran and Laurentide ice sheets grew on North America and coalesced along an approximately 1500-km-long suture zone over the eastern foothills of the Canadian Cordillera (Fig. 1A and B) (Jackson et al., 1997; Dyke, 2004; Dalton et al., 2020), constituting the largest ice mass and contributor to post-LGM sea-level change on the planet (Tarasov and Peltier, 2005; Clark et al., 2009; Tarasov et al., 2012; Lambeck et al., 2014, 2017). Deglacial retreat of these ice sheets was underway for most of their margins by ~19 ka (ka = kilo annum) (Clark et al., 2009). As

deglaciation proceeded, global mean sea level (GMSL) rose, punctuated by a rapid 9–16 m rise in GMSL $\sim\!14.6\text{-}14.3$ ka (Deschamps et al., 2012; Liu et al., 2016) called Meltwater Pulse 1A (MWP-1A). A proposed causal mechanism for this meltwater pulse is the collapse and ultimate separation of the saddle where the Cordilleran and Laurentide ice sheets coalesced (Fig. 1A) (Gregoire et al., 2012, 2016; Gomez et al., 2015; Lambeck et al., 2017; Lin et al., 2021; Stoker et al., 2022), whereby initial lowering of the ice saddle initiates positive surface mass balance feedbacks that lead to accelerated ice-sheet mass loss (Carlson et al., 2009). Thus, a saddle collapse constitutes a potential instability in the conjoined Cordilleran-Laurentide ice sheets that could produce an

E-mail addresses: areyes@ualberta.ca (A.V. Reyes), d.rood@imperial.ac.uk (D.H. Rood).

https://doi.org/10.1016/j.quascirev.2024.108554

^{*} Corresponding author.

^{**} Corresponding author.

abrupt rise in GMSL like MWP-1A (Tarasov and Peltier, 2005; Tarasov et al., 2012; Gregoire et al., 2012), particularly if it was triggered by abrupt climate warming (Gregoire et al., 2016; Stoker et al., 2022). Indeed, MWP-1A occurred during the Northern Hemisphere Bølling warm period of ~14.7–14.1 ka (Rasmussen et al., 2006; Clark et al., 2012; Deschamps et al., 2012).

Testing the above hypothesis and assessing the overall role of the saddle collapse in sea-level rise (Tarasov and Peltier, 2005; Tarasov et al., 2012; Gregoire et al., 2012, 2016; Gomez et al., 2015; Liu et al., 2016; Stoker et al., 2022) requires improved constraints on the timing of Cordilleran-Laurentide ice-sheet separation. Existing chronologies rely on minimum-limiting age constraints, many of which include large, millennial-scale uncertainties (Froese et al., 2019). Here, we consider 64 10 Be surface exposure ages at six locations spanning \sim 1200 km of the Cordilleran-Laurentide suture zone (Fig. 1A) that provide the first direct dating of when these two ice sheets separated completely. Our six sampling sites are located along a south-north transect from ${\sim}50^{\circ}N$ to ~59°N where mapping places the confluence of the two ice sheets (Fig. 1B) (e.g., Bobrowsky and Rutter, 1992; Catto et al., 1996; Jackson et al., 1997; Dyke, 2004; Bednarski and Smith, 2007; Hartman and Clague, 2008; Atkinson et al., 2016; Hickin et al., 2016; Huntley et al., 2016; Utting et al., 2016; Hartman et al., 2018; Dalton et al., 2020), thus providing chronological control on the end of the separation event in the suture zone. These ¹⁰Be ages were also reported in Clark et al. (2022) but with respect to when an ice-free corridor formed that could be utilized for human migration to south of the Cordilleran-Laurentide ice sheets. Here we discuss these 64 ¹⁰Be ages with respect to the retreat of these ice sheets and their attendant contribution to sea-level rise and MWP-1A.

2. Methods

2.1. Field sampling

We collected samples for ¹⁰Be surface exposure ages at six sites: ABS, ABC, ABN, BCS, BCC, and BCN (Fig. 1A). At five of our sites, ABS, ABC, ABN, BCS, and BCC, we collected samples from boulders on bedrock. At our sixth, northernmost site (BCN), we collected a mixture of boulderon-bedrock samples and glacier-scoured bedrock samples. Sampling followed prior methods used to document ice-sheet-scale changes in ice margins and ice area (Cuzzone et al., 2016; Ullman et al., 2016). Each of these sites is located near the mapped confluence of the Cordilleran-Laurentide ice sheets (Fig. 1) (Bobrowsky and Rutter, 1992; Catto et al., 1996; Jackson et al., 1997; Dyke, 2004; Bednarski and Smith, 2007; Hartman and Clague, 2008; Atkinson et al., 2016; Hickin et al., 2016; Huntley et al., 2016; Utting et al., 2016; Hartman et al., 2018; Dalton et al., 2020). The final location of the suture zone just prior to separation is difficult to identify as this zone shifted during the last glaciation (Hartman and Clague, 2008; Atkinson et al., 2016; Hickin et al., 2016; Huntley et al., 2016; Utting et al., 2016; Hartman et al., 2018). Potential cover by proglacial lakes following deglaciation is another complication to site selection (Lemmen et al., 1994; Utting and Atkinson, 2019). In all cases, care was taken to sample above any proglacial lakes. In some cases, glacial lakes necessitated site modification from the location with the simplest deglacial history. In the end, each site was chosen for the simplest deglacial history in that region that also had continuous exposure of the sampled surface since ice-sheet deglaciation.

By sampling boulders on bedrock, or the bedrock itself, we avoid potential issues of buried ice melting and causing reworking of boulder samples after regional deglaciation. As all of our sampled boulders are directly on bedrock, we minimize potential concerns from prior till erosion shifting or exposing parts of the boulder surface. Similarly, we

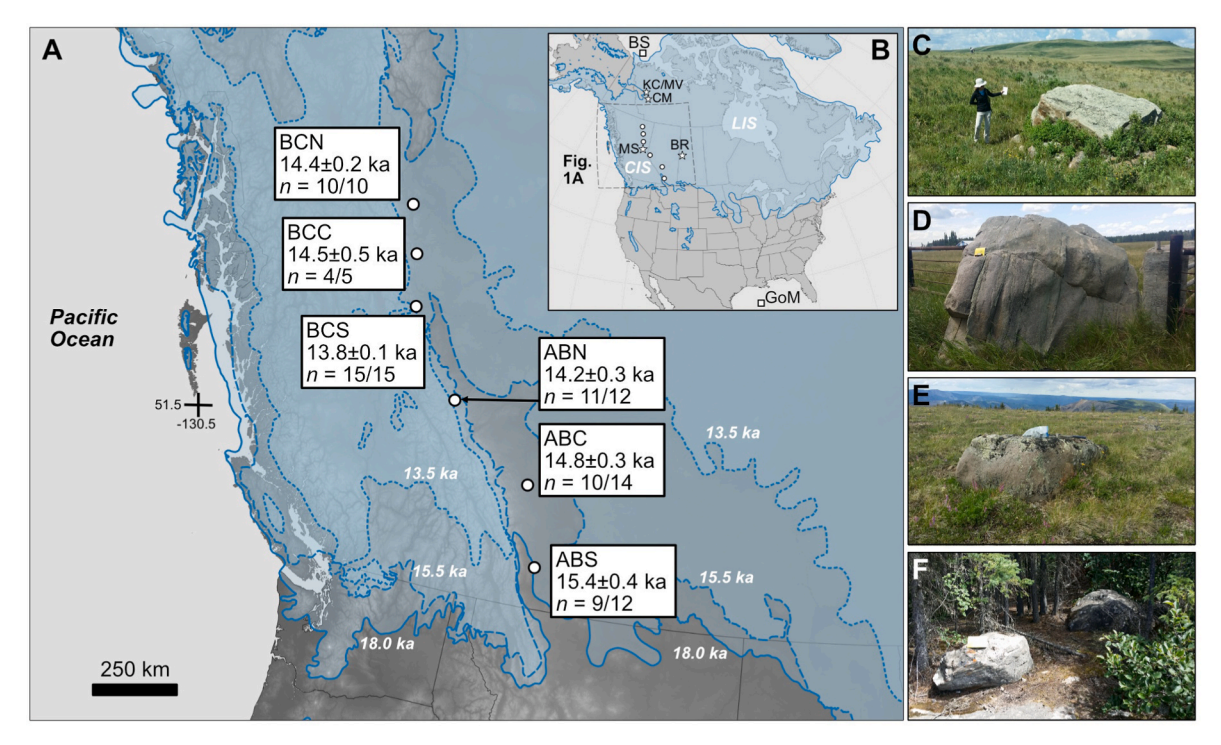


Fig. 1. Cordilleran-Laurentide suture zone maps and example boulder sites. (A) Suture zone map showing our site locations with mean ¹⁰Be ages and number of samples (n). Map ice-margins (Dalton et al., 2020) are in calibrated ka. (B) Cordilleran (CIS) and Laurentide (LIS) ice sheets at their ~18 ka extent (Dalton et al., 2020). Marine core locations indicated by open squares in the Gulf of Mexico (GoM; Wickert et al., 2013) and Beaufort Sea (BS; Keigwin et al., 2018). Locations of Stoker et al. (2022) ¹⁰Be ages noted by two stars: southern is Cap Mountain (CM); northern is Katherine Creek (KC) and Mackenzie Valley (MV). Locations of the Norris et al. (2022) Beaver River (BR) sample site and Dulfer et al. (2021) Mount Spieker (MS) site noted by stars. (C–F) Examples of boulders at sites ABS (C), ABC (D), ABN (E), and BCS (F).

found no evidence of till cover of the sampled bedrock surfaces, minimizing potential exhumation of the surface after deglaciation.

Our Alberta sample sites are shown in Fig. 2. ABS is the southernmost site (50.1° N, 113.8° W, \sim 1200 m above modern sea level). It consists of isolated quartzite and quartzose sandstone boulders resting on uplifted bedrock of the Canadian Rockies foothills. These boulders comprise the Foothills erratics train that was deposited by Cordilleran ice flowing out of the mountains that was then directed southwards by confluence with the Laurentide ice sheet (Stalker, 1956; Jackson et al., 1997). We collected 10 samples from this sample site and include two additional ages from Margold et al. (2019) (ALT-MM-15-08, ALT-MM-15-09) that were collected nearby our samples. A meltwater channel (or possibly a subglacial tunnel channel; Rains et al., 2002) is incised into the bedrock to the west of many of our samples; we made sure to sample above this channel

Site ABC also consisted of quartzite boulders from the erratics train but is located farther to the east of the Rocky Mountains on the piedmont (52.2°N, 114.8°W, \sim 1100 m above modern sea level) near the village of Chedderville, AB. Here the boulders are isolated and resting on the poorly consolidated bedrock of the piedmont surface. We collected 12 samples at ABC and combined them with two ages of Margold et al. (2019) (ALT-MM-15-14, ALT-MM-15-15).

We interpret the exposure ages from sites ABS and ABC as constraints on the timing of Cordilleran-Laurentide ice-sheet separation, following Jackson et al. (1997), Margold et al. (2019) and Norris et al. (2022). Since the boulders sampled at these two sites were transported by the Cordilleran ice sheet, their exposure occurred shortly after the two ice sheets separated as the Cordilleran ice sheet retreated. Our

interpretation is compatible with the work of Utting et al. (2016) who reconstructed continued Cordilleran ice-sheet retreat after separating from the Laurentide ice sheet to the northwest of ABC.

ABN is located in the eastern foothills of the central Canadian Rockies (54.0°N, 119.0°W, ~1800 m above modern sea level). We sampled 12 sandstone boulders located on two bedrock ridges near Grande Cache, AB. Four samples are from an unnamed foothill northeast of Grande Cache at ~1700 m (54.0°N, 118.9°W). Another eight samples are from near the summit of Grande Mountain just north of Grande Cache (53.9°N, 119.1°W, \sim 1890–1960 m). These sites face one another on either side of the Muskeg River valley and are to the west of the mapped confluence of the two ice sheets, which shifted during the glacial maximum (Atkinson et al., 2016). Sampling closer to the confluence was not possible due to potential proglacial lake coverage. Given the similar elevations on either side of this valley, they should both date thinning of ice below these ridges as the Cordilleran ice sheet transitioned to flow being directed by local topography (Atkinson et al., 2016). Atkinson et al. (2016) mapped such flow patterns in this region, identifying two sets of flow at site ABN: a pattern that flowed over the tops of the ridges during Cordilleran ice-sheet expansion as it built up to its confluence with the Laurentide ice sheet (i.e., pre-maximum extent) and a flow pattern where ice was constricted to valleys after the separation of the two ice sheets. This latter flow pattern is only noted up to a modern elevation of ~1420 m while our ridge sampling sites are above this elevation. As such, the two ABN sites should date the thinning of ice just prior to its transition to this valley-controlled flow pattern that occurred immediately after ice-sheet separation according to Atkinson et al. (2016). Accordingly, ABN constrains the ice-sheet separation,

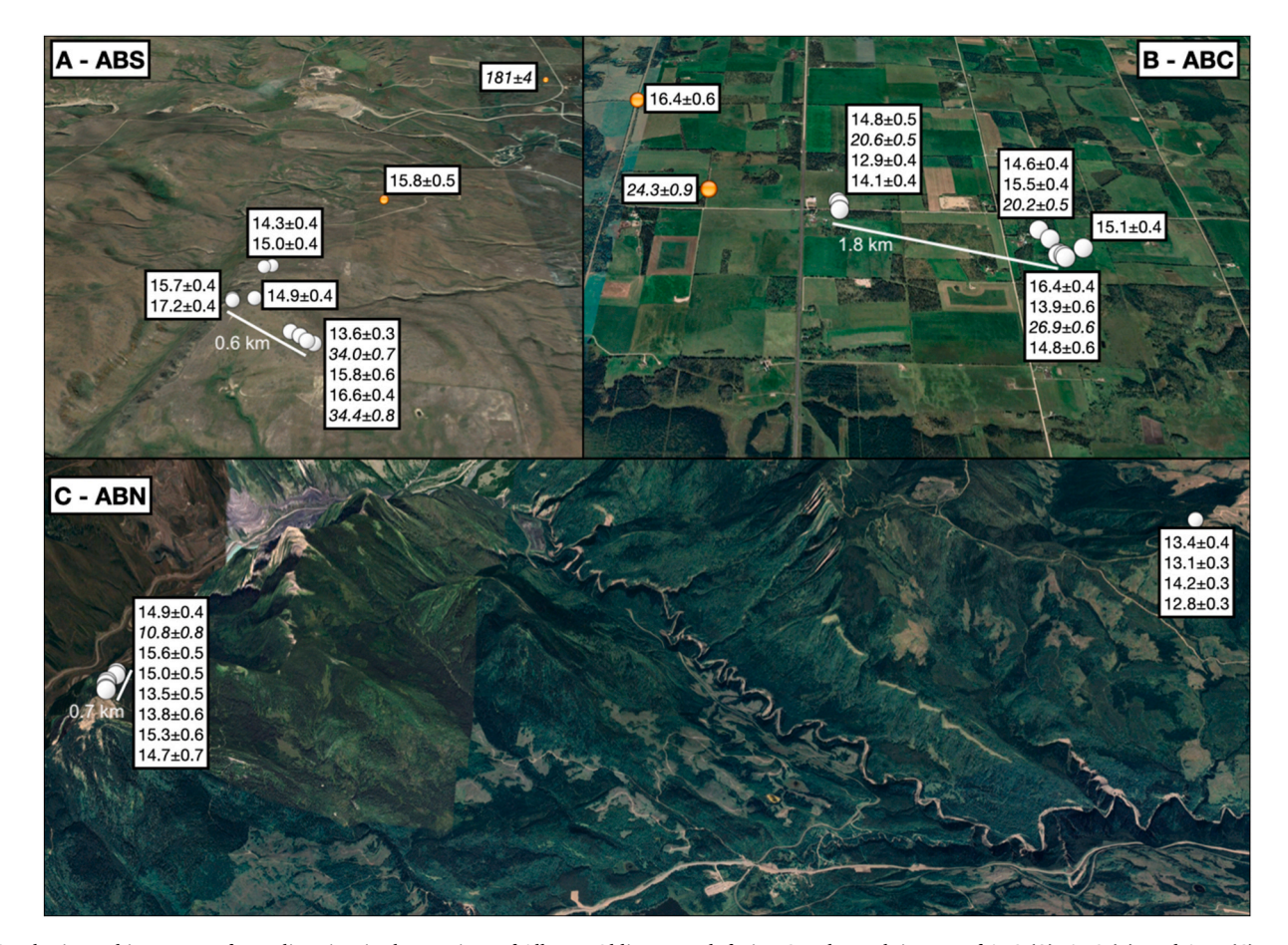


Fig. 2. Physiographic context of sampling sites in the province of Alberta. Oblique, north-facing Google Earth images of ABS (A), ABC (B), and ABN (C) sampling sites with three times vertical exaggeration. White symbols show our sample locations; yellow symbols represent sample locations and ages from Margold et al. (2019). White lines provide scale to the oblique imagery. Uplift-corrected ¹⁰Be ages with analytical uncertainty noted in ka. Numbers in italics indicate outlier ages excluded from calculation of the sample mean and uncertainty.

because the two ridges became exposed in the last stages of ice-sheet separation to just after this separation. Note that Atkinson et al. (2016) mapped this separation as not progressing northwards like an unzipping but rather occurring in a fashion that left local ice-free regions entirely surrounded by ice.

Our British Columbia sample sites are shown in Fig. 3. BCS is located west of Hudson Hope, BC on a bedrock ridge that comprises Bullhead Mountain (56.1°N, 122.2°W, ~1100 m above modern sea level). The sandstone ridge is the easternmost surface expression of the Rocky Mountains and forms the northeast shore of Williston Lake. We sampled 15 sandstone boulders resting on bedrock. BCS is a well-studied region. Catto et al. (1996), Hartman and Clague (2008), Hickin et al. (2016), and Hartman et al. (2018) mapped the glacial geomorphology and stratigraphy of this region. Catto et al. (1996) mapped Laurentide ice-sheet-transported erratics as far west as our sample site at Bullhead Mountain, meaning BCS was at some point underneath the Laurentide ice sheet. Hartman and Clague (2008) came to the same conclusion and also inferred that BCS could be the suture zone of Cordilleran-Laurentide ice sheets. Hartman and Clague (2008) also recognized a subsequent readvance or stillstand of the Cordilleran ice sheet after separation from the Laurentide ice sheet. To the south of BCS, Hickin et al. (2016) determined that a Cordilleran ice-sheet advance extended eastward of the Rocky Mountains and contacted the Laurentide ice sheet. Hartman et al. (2018) examined this evidence and found that this eastward advance occurred prior the advance of the Laurentide ice sheet up to the Rocky Mountains that constituted the confluence of the two ice sheets, although they could not rule out a later eastward movement of the ice-sheet suture zone to the east of BCS. Thus, the Laurentide ice sheet advanced to the location of BCS during ice-sheet confluence but it remains unclear if the confluence zone remained over BCS after conjoining or shifted eastward prior to separation. After ice-sheet separation, the Cordilleran ice sheet readvanced eastward to just east of Bullhead Mountain where the Portage moraine was deposited (Catto et al., 1996; Hartman and Clague, 2008; Hartman et al., 2018). This moraine is at ~700 m above modern sea level. We explicitly chose BCS at ~1100 m above modern sea level on a bedrock ridge that rises above the moraine. At this elevation, BCS is also above Glacial Lake Peace that formed against the Laurentide ice sheet after ice-sheet separation. As such, the BCS samples are from the location that would most closely date the timing of ice-sheet separation in this region prior to this Cordilleran ice-sheet readvance but also not be submerged by Glacial Lake Peace.

BCC is on a foothill bedrock ridge east of the Canadian Rockies (57.5°N, 122.9°W, $\sim\!1200$ m above modern sea level). We found only five coarse-grained sandstone boulder samples at this site. While the precise location of the Cordilleran-Laurentide ice-sheet confluence is not directly mapped in this region, Bednarski and Smith (2007) mapped Laurentide-sourced erratics in the Cordilleran foothills. Our five samples come from a ridge $\sim\!10$ km to the east of these Laurentide erratics and are west of glacial flutings that show west-southwest Laurentide ice-sheet flow (Bednarski and Smith, 2007). We interpret the age of our samples as dating retreat of the Laurentide ice sheet as, or just after, it separated from the Cordilleran ice sheet.

BCN is on a sandstone ridge that rises to Tepee Mountain (58.7°N, 123.8° W, ~ 1000 m above modern sea level). Like BCC, we found only four sandstone boulders to sample (BCN-4-16, BCN-5-16, BCN-7-16, BCN-8-16), which we supplemented with an additional six sandstone bedrock samples to give a total of 10 samples. The sandstone boulders are sourced from the local sandstone bedrock. BCN is the least studied sampling site of the six. Bobrowsky and Rutter (1992) summarized mapping of the ice-sheet suture zone and found consistent placement of



Fig. 3. Physiographic context of sampling sites in the province of British Columbia. Oblique, north-facing Google Earth images of BCS (A), BCC (B), and BCN (C) sampling sites with three times vertical exaggeration. White lines provide scale to the oblique imagery. Uplift-corrected ¹⁰Be ages with analytical uncertainty noted in ka. Numbers in italics indicate outlier ages excluded from calculation of the sample mean and uncertainty. Ages marked with an asterisk were obtained from a bedrock sample.

this zone slightly to the west of BCN. Dyke (2004) maintained this confluence location just to the west of BCN. Huntley et al. (2016) mapped the confluence of the Cordilleran-Laurentide ice sheets north of 59°N, and thus north of BCN. Extrapolating the southeast trend of their location for ice-sheet separation southward from 59°N to 58.7°N places BCN very close to, if not at, the location where the two ice sheets separated. We propose that the BCN exposure ages closely constrain the separation of the Cordilleran-Laurentide ice sheets, dating when the Laurentide retreated shortly after it separated from the Cordilleran ice sheet, if not the precise timing of ice-sheet separation.

2.2. ¹⁰Be target preparation and measurement

Thirty-four samples were prepared at PRIME Laboratory at Purdue University (6 = ABS, 8 = ABC, 5 = ABN, 5 = BCS, 5 = BCC, 5 = BCN). These samples were physically and chemically separated with ¹⁰Be concentration measured by AMS at PRIME Lab of Purdue University following standard techniques (www.physics.purdue.edu/primelab/). The samples were first crushed and sieved to obtain a 250-500 µm sizefraction. Magnetic and density separations were used to reduce nonquartz minerals. The final quartz purification was done by chemical etching using procedures described in Kohl and Nishiizumi (1992). Quartz purity was tested by ICP-OES prior to digestion. Following purification, the quartz was dissolved in the presence of a low background ⁹Be carrier (10 Be/ 9 Be < 10^{-15}). The purified BeO was loaded into stainless steel cathodes and analyzed following the procedures outlined in Sharma et al. (2000). All measured ¹⁰Be/⁹Be ratios were normalized to primary standards (10 Be/ 9 Be = 2850 \times 10 $^{-15}$) prepared by K. Nishiizumi (Nishiizumi et al., 2007). The ratios, samples masses, carrier amounts, and blank correction are shown in Table S1.

Another 30 samples were prepared at CosmIC Laboratories at Imperial College London (4 = ABS, 4 = ABC, 7 = ABN, 10 = BCS, 0 = BCC, 5 = BCN) using standard procedures (Corbett et al., 2016). Following isolation, the final purity of the quartz and beryllium, and high yield of beryllium, were all verified using an Agilent 5100 SVDV ICP-OES. Beryllium oxide was mixed with niobium in a 1:1 M ratio and packed into copper cathodes for ¹⁰Be/⁹Be isotopic analysis by AMS on the 6 MV Sirius tandem accelerator in the Center for Accelerator Science at ANSTO (Wilcken et al., 2017). Data were normalized to the KN-5-3 standard with a reported $^{10}\text{Be}/^{9}\text{Be}$ ratio of 6.32×10^{-12} , respectively, which is consistent with the revised ¹⁰Be decay constant (Nishiizumi et al., 2007). Secondary standards produced by K. Nishiizumi were run as unknowns to confirm the linearity of the isotopic measurements. A full process blank (Be carrier only) was processed with each batch of samples. Analyses were corrected for backgrounds with uncertainties in sample and batch-specific blank propagated in quadrature (Table S2). The ¹⁰Be backgrounds represent a small portion (0.5–1.8%) of the measured total 10Be atoms in the samples. Isotopic ratio data were reduced to isotope concentrations considering the measured isotopic ratios, the background correction, the mass of quartz dissolved, and the total ⁹Be carrier added to the sample (Table S2). Replicate preparations and analyses of two quartz samples (ABS-9-16 and ABS-9-16R, and BCN-11-16 and BCN-11-16R, respectively) both reproduced within their 1σ uncertainties (Table S2).

2.3. Age calculation and isostatic rebound

We calculated 10 Be ages using the Lal/Stone time-varying scaling using the CRONUS-Earth online calculator (Balco et al., 2008) and the non-uplift-corrected Arctic 10 Be production rate (Young et al., 2013) (Tables S3 and S4). Use of another scaling (LSD; Lifton et al., 2014) does not change our results or conclusions (average absolute difference in age is 70 years; average relative age difference is 0.5%). We chose the non-uplift corrected Arctic production rate as it is applicable to exposure age sites from $>40^{\circ}$ N and up to 1000 m above sea level (Young et al., 2013). Our sampling sites are all north of 40° N and currently average

 $\sim\!1200$ m in elevation, close to 1000 m. While 1200 m is above 1000 m, the Artic production rate is the geographically closest production rate to our sampling sites.

We did not apply the Young et al. (2013) uplift correction to the Arctic production rate, because Young et al. (2013) recommended using the non-uplift-corrected rate. Specifically, Young et al. (2013) found that the non-uplift-corrected production rate better fit calibration datasets and that it agreed with the one calibration set that had experienced the least amount of uplift. In contrast, Young et al. (2020) suggested that if a cosmogenic nuclide sampling site is uplift corrected, then the production rate site should be uplift corrected if it has undergone isostatic rebound. However, we do not use the uplift-corrected Arctic production rate for two reasons: 1) the Arctic production rate currently lacks an appropriate uplift correction, and 2) any such uplift correction is small and within the uncertainty of the production rate.

The Arctic production rate comes from coastal moraine boulders or ice-contact delta boulders in Baffin Bay, Norway, and New England, with three landslide sites in Norway that postdate glaciation by varying degrees. These production rate sites are near the maximum limits of ice sheets where the ice margins were much thinner than in the interior of the North American ice-sheet complex (e.g., Peltier, 2004; Tarasov et al., 2012; Lambeck et al., 2017). As such, these coastal regions experienced significantly less uplift/reduction in atmospheric depth than at our sample sites near the center of the North American ice-sheet complex (e. g., Peltier, 2004; Tarasov et al., 2012; Lambeck et al., 2017). Consequently, the uplift correction is more important to sites in the interior of ice sheets than for sites near coastlines. The site-specific uplift corrections for the Arctic production rate were calculated using relative sea-level change at the production rate sites in Baffin Bay and Norway, excluding the youngest middle Holocene landslide site. Using relative sea-level change includes additional effects such as gravitational attraction of the ice sheet and changing barystatic sea level (Farrell and Clark, 1976), which do not influence the change in atmospheric depth at the site (Carlson, 2020).

The uplift correction used by Young et al. (2013) for the New England production rate sites was from Balco et al. (2009), who correctly calculated the change in atmospheric depth from uplift in the ICE-5G model (Peltier, 2004). Balco et al. (2009) also calculated the change in atmospheric depth at one of the Baffin Bay production rate sites. We can thus test the impact of an uplift correction on the Arctic production rate. Balco et al. (2009) found that uplift would increase production rates by $1.5\%{-}2.5\%$, with the latter being the correction for the Baffin Bay site. Adopting the larger value (2.5%) shifts the Arctic production rate from 3.96 atoms g^{-1} yr $^{-1}$ to 4.06 atoms g^{-1} yr $^{-1}$, which is within the ± 0.15 atoms g^{-1} yr $^{-1}$ uncertainty of the Arctic production rate without an isostatic uplift correction (applying the 1.5% correction to the New England sites shifts the mean even less).

Several recent studies have corrected their sampling sites from near the center of the North American ice-sheet complex for isostatic uplift (i. e., Dulfer et al., 2021; Stoker et al., 2022; Norris et al., 2022) and then used the global production rate of Borchers et al. (2016) to determine exposure age. This global production rate estimate includes sites from >40°N (Puget Sound U.S.A., Scotland, New England, U.S.A., and two sites in Norway). These regions were under ice sheets during the last ice age and have undergone isostatic uplift since deglaciation. However, Borchers et al. (2016) did not correct these sites for uplift. A correction would vary greatly between the Isle of Skye, Scotland, where the Younger Dryas re-advance after ice-sheet recession was limited, to New England or Norway, which were covered by continental-scale ice sheets. This spread in uplift correction is similar to that for the Arctic production rate, which includes sites from under three different ice sheets, two sites that shortly postdate glaciation, and a site from the middle Holocene. Borchers et al. (2016) observed agreement within these measurement areas from around the globe and determined not to attempt an uplift correction. This supports our above assessment that the uplift correction at production rate sites from the maximum limit of ice sheets is small and within the uncertainty. These uncertainties are also built into the CRONUS calculators. Like other factors that influence cosmogenic nuclide concentrations, e.g. production rates, prior exposure, etc., uplift differences between the calibration sites would account for dispersion in nuclide concentrations; the uncertainties provided by the CRONUS calculator reflect these. Given the current precision of exposure age determinations, an uplift correction would be "in the noise" of other sources of uncertainty.

The Cordilleran-Laurentide ice-sheet suture zone, on the other hand, has undergone extensive isostatic rebound following deglaciation (e.g., Tarasov et al., 2012; Lambeck et al., 2017), which in certain settings, like in the interior of an ice sheet where significant isostatic depression occurred, should be accounted for when calculating surface exposure ages (e.g., Cuzzone et al., 2016; Ullman et al., 2016; Leydet et al., 2018; Carlson, 2020; Dulfer et al., 2021; Clark et al., 2022; Norris et al., 2022; Reyes et al., 2022; Stoker et al., 2022). Our approach for the cosmogenic nuclide data interpreted here has been previously discussed in Reyes et al. (2022) and Clark et al. (2022). Briefly, we generated new uplift histories at our data sites for the ANU ice history and nine Earth viscosity models that span the range of uncertainty in the Earth model parameters as determined by Lambeck et al. (2017). However, the Lambeck et al. (2017) uplift history has a set ice-margin history, which is not consistent with the six means and uncertainties of ¹⁰Be ages we calculate using the above discussed production rate and scaling methodology (with outliers removed - see below). That is, we date deglaciation before the region becomes ice-free in the Lambeck et al. (2017) model even when using the Lambeck et al. (2017) uplift correction.

We therefore generated two new simulations using the ice-sheetsystem model of Tarasov et al. (2012) forced with a modified ice-limit chronology based on our ¹⁰Be ages with the Lambeck et al. (2017) uplift correction. (Note that this ice-margin modification extends northwards to the study area of Reyes et al. (2022) for the northwestern Laurentide ice-sheet margin.) Specifically, the Tarasov et al. (2012) model simulations have a component that adjusts the surface mass balance within climatic uncertainties to nudge the simulation towards consistency with the uncertainty bounds of the Dyke (2004) deglacial chronology. We modified the Dyke (2004) chronology to match ¹⁰Be ages we calculated using the Lambeck et al. (2017) uplift and ran two simulations with the modified forcing (nn3135, nn3136). Runs nn3135 and nn3136 are respective variants of the reasonable fit nn9894 and nn9927 ensemble members from the data-calibrated glaciological modelling of Tarasov et al. (2012) with the same glacial systems model parameter vectors but with a temporally advanced ice-margin nudging chronology. The advance was imposed after 14.58 ka and before 8.34 ka to have the Cordilleran-Laurentide separation be in approximate accord with the new ages presented herein. We then used nn3135 and nn3136 to calculate new isostatic uplift histories based on the VM5a Earth viscosity model (Peltier and Drummond, 2008), which was used in their development (Table S5). This iterative process results in a more self-consistent analysis. Namely, the unloading history from ice-sheet thinning, the rebound of the underlying bedrock and the timing of deglaciation determined by the 10Be ages are all consistent with one another.

We do not correct for changes in atmospheric pressure caused by changes in ice-sheet dimensions (e.g., Staiger et al., 2007). Prior analyses in general circulation models of the change in atmospheric pressure since deglaciation at cosmogenic sampling sites similar to ours (central and eastern Canada, Scandinavia) found negligible impacts on the cosmogenic exposure age once the total time since deglaciation was assessed (Cuzzone et al., 2016; Ullman et al., 2016; Leydet et al., 2018). While there is an initial atmospheric pressure difference (Staiger et al. (2007), this impact quickly dissipates as the ice sheet recedes and becomes inconsequential once the entire atmospheric pressure change is considered since deglaciation (Cuzzone et al., 2016; Ullman et al., 2016; Leydet et al., 2018).

Following Margold et al. (2019), Stoker et al. (2022), and Norris

et al. (2022), we do not correct for snow cover impacts on cosmogenic nuclide surface exposure age. While Dulfer et al. (2021) did apply such a correction to their Mount Spieker ¹⁰Be ages, they noted that such a correction was highly uncertain, particularly given the potential impacts of early to middle Holocene warmth on snow cover. As this constitutes a known unknown, we do not apply such a correction but do note the potential impact of snow cover that would shift our ¹⁰Be ages older. We also did not correct for any vegetation cover of the samples.

After including four 10 Be ages from Margold et al. (2019) at ABS and ABC, we calculated site-specific average deglacial ages following the methods of Cuzzone et al. (2016) and Ullman et al. (2016). While Margold et al. (2019) contains additional 10 Be ages elsewhere along the Foothills erratics train, these typically consisted of one or two isolated boulders that are not appropriate for averaging to obtain a deglaciation age at a given site. We opted to include only those samples that were near our sites with multiple sampled boulders at one locality (i.e., $n \geq 3$ after outlier removal). We first identified outliers using the most basic and conservative understanding of the deglacial chronology of the region. Apparent old sample dates were flagged by being >19 ka in age and thus from at least the LGM when the region clearly was not ice free. Ages from the Holocene (<11.7 ka) were flagged as being young outliers.

Following exclusion of these nine outlier samples, we determined the mean and uncertainty for site deglaciation using either the arithmetic mean and standard error or the error-weighted mean and uncertainty, choosing the method that results in the greater uncertainty of the mean (Cuzzone et al., 2016; Ullman et al., 2016). This is a conservative approach as it maximizes the uncertainty in the estimated timing of deglaciation. In all cases, except for the existing data of Norris et al. (2022) (see below), the arithmetic mean and standard error resulted in the larger uncertainty and is what we present here.

We also recalculated 15 of the 23 10 Be ages from Stoker et al. (2022) and four of the eight ¹⁰Be ages from Dulfer et al. (2021) using the same uplift correction methods as employed for our ¹⁰Be ages and the Arctic production rate (Table S3). The 15 ages of Stoker et al. (2022) are from three sites that have at least three samples per site (Fig. 1B). We find that greater uplift occurred in our new ice-sheet model simulations than was used by Stoker et al. (2022). This is not surprising as our simulations are optimized to match an earlier deglaciation chronology found in the ¹⁰Be ages whereas Stoker et al. (2022) used Lambeck et al. (2017) that relied on the younger radiocarbon-based deglacial chronology that is now shown to be too young for the northwestern Laurentide ice sheet (Reves et al., 2022). The four Dulfer et al. (2021) ages are from their eastern sampling site on the summit of Mount Spieker in the eastern Canadian Rockies (Fig. 1B). Our methodology reproduces the same ages as Dulfer et al. (2021) reported but without necessitating the use of a snow-cover correction.

We also include six of the 26 ¹⁰Be ages from Norris et al. (2022). These are from their westernmost site in western Saskatchewan on the Beaver River, providing the westernmost direct deglacial age control for the southwestern Laurentide ice-sheet margin after separation from the Cordilleran ice sheet (Fig. 1B). The six ages come from two sites \sim 30 km apart along the Beaver River, with four ages at the eastern location and two more at the western location. Norris et al. (2022) combined them into a regional deglaciation age, which we also do here. For these six ages, we use the Arctic production rate as applied to the other ages, but we do not use the uplift correction from the two new ice-sheet model simulations. This is because the Norris et al. (2022) site is ~500 km east of our sampling sites and the ice-sheet suture zone. This is well outside the region where we tuned the ice-sheet model. As such, it is unknown how our localized ice-margin tuning would impact the model deglacial history at the Norris et al. (2022) site. Thus, we use the uplift correction that Norris et al. (2022) determined from the ice-sheet model simulations of Tarasov et al. (2012).

2.4. Sea-level rise calculation

To calculate the contribution to global mean sea level (GMSL) rise from Cordilleran-Laurentide ice-sheet separation, the zone of separation in which the saddle collapse occurred must be defined (Gregoire et al., 2012). In a dynamic ice-sheet model, this is extremely difficult to define as ice divides migrate, making the saddle region vary as the saddle collapse occurs. As such, we chose a region that encompasses the suture zone, as in Gregoire et al. (2012), and calculated ice-volume changes within this region. The region is defined by the boundaries 50-65°N and 105-125°W. We used 500-year time steps of ice thickness that are reduced to 100-year time steps during the MWP-IA time window of 14.7-14.0 ka, when calculating the volume changes in output from model runs nn3135 and nn3136 (Table S5). We acknowledge that the 100-year temporal resolution equals or exceeds the reliable temporal resolution of the ¹⁰Be dates for deglaciation. The ice volume changes were then converted to barystatic GMSL changes based on the present-day surface area of the ocean (Tarasov et al., 2012).

3. Results and discussion

3.1. 10Be ages

Nine samples from the full 68 sample dataset, two of which are from Margold et al. (2019), were identified as outliers (Fig. 4; Table S3). Note that uplift corrections were applied to all samples including those later determined to be outliers. Uplift corrections increased from south to north (Table S3), reflecting increasing ice-sheet loading (e.g., Peltier, 2004; Tarasov et al., 2012; Lambeck et al., 2017). ABS had a correction of -24 m, ABC -42 m, ABN -55 m, BCS and BCC -80 m, and BCN had a correction of -84 m. Uncertainties in the site means are presented as the internal standard error, with external uncertainty that includes the

¹⁰Be-production rate uncertainty (Young et al., 2013) noted in parentheses below.

At ABS, samples ABS-6-16 (34.0 \pm 0.7 ka), ABS-8-16 (34.4 \pm 0.8 ka), and ALT-MM-15-09 (181 \pm 4 ka) were identified as outliers that likely contained ^{10}Be from pre-last deglaciation exposure of the boulder surface (Fig. 4A). The arithmetic mean and standard error for deglaciation at ABS is 15.4 \pm 0.4 (0.7) ka (n = 9, 3 outliers) (Fig. 5C). Given the location of ABS and it being covered by the Cordilleran ice sheet, we interpret its ice-free timing as indicating ice-sheet separation was underway by $\sim\!15.4$ ka.

At ABC, samples ABC-11-16 (20.6 \pm 0.5 ka), ABC-7-16 (26.9 \pm 0.6 ka), ABC-8-16 (20.2 \pm 0.5 ka) and ALT-MM-15-14 (24.3 \pm 0.9 ka) were identified as outliers that likely contained ^{10}Be from pre-last deglaciation exposure of the boulder surface (Fig. 4B). Deglaciation at ABC concluded at 14.8 \pm 0.3 (0.6) ka (n = 10, 4 outliers) (Fig. 5C). Similar to ABS, we take the ABC deglaciation age to indicate on-going ice-sheet separation at $\sim\!14.8$ ka.

One young sample at ABN (ABN-10-16, 10.8 ± 0.8 ka) in the western subgroup was identified as an outlier (Fig. 4C), that probably reflects post-depositional movements of the boulder, leading to our sampling of a surface that was not horizontal for an unknown period following deglaciation. The eight western samples at ABN date to 14.3 ± 0.3 ka (n = 7, 1 outlier) whereas the eastern samples at ABN date to 13.4 ± 0.3 ka (n = 4, no outliers). While these two sites are ~15 km apart, they are at similar elevations and are located on opposite sides of the same valley. Based on the flow patterns of Atkinson et al. (2016) and due to their across-valley setting, these two locations should yield similar ages for Cordilleran ice-sheet thinning as it transitioned to flow constrained by local topography in the last stages of separation to just after its separation from the Laurentide ice sheet. The eight western sample ages span from 15.6 ± 0.5 ka to 13.5 ± 0.5 ka while the eastern ages span from 14.2 ± 0.3 ka to 12.8 ± 0.3 ka. Determining if they are truly different in

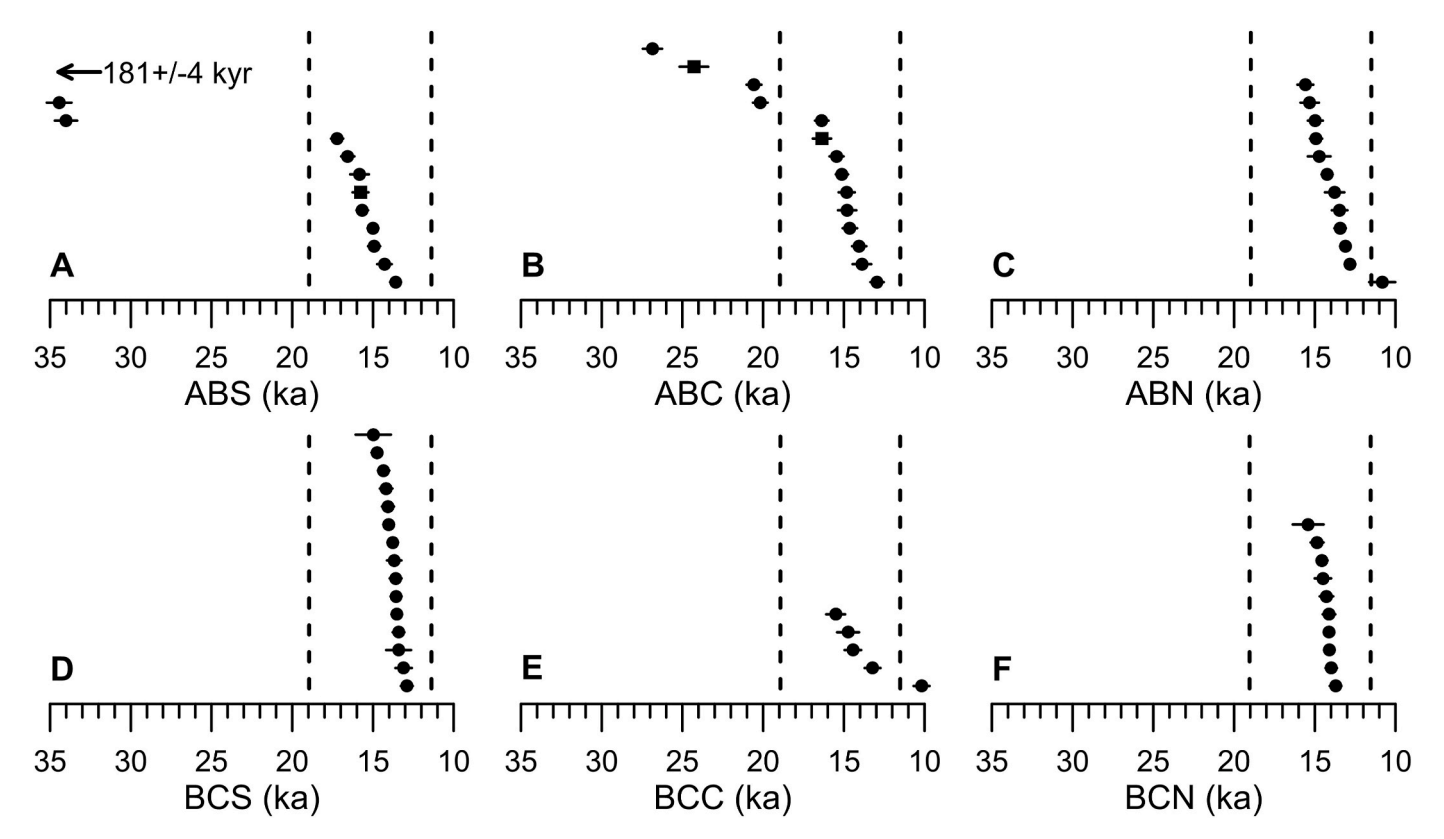


Fig. 4. ¹⁰Be age results. A, ABS (50.1°N); B, ABC (52.2°N); C, ABN (54.0°N); D, BCS (56.1°N); E, BCC (57.5°N); F, BCN (58.7°N). Vertical dashed lines denote outlier exclusion limits for the last glacial maximum (>19.0 ka) and the Holocene (<11.7 ka) (Rasmussen et al., 2006; Clark et al., 2009). Our samples are circles; squares are from Margold et al. (2019). Horizontal bars are 1σ analytical uncertainty.

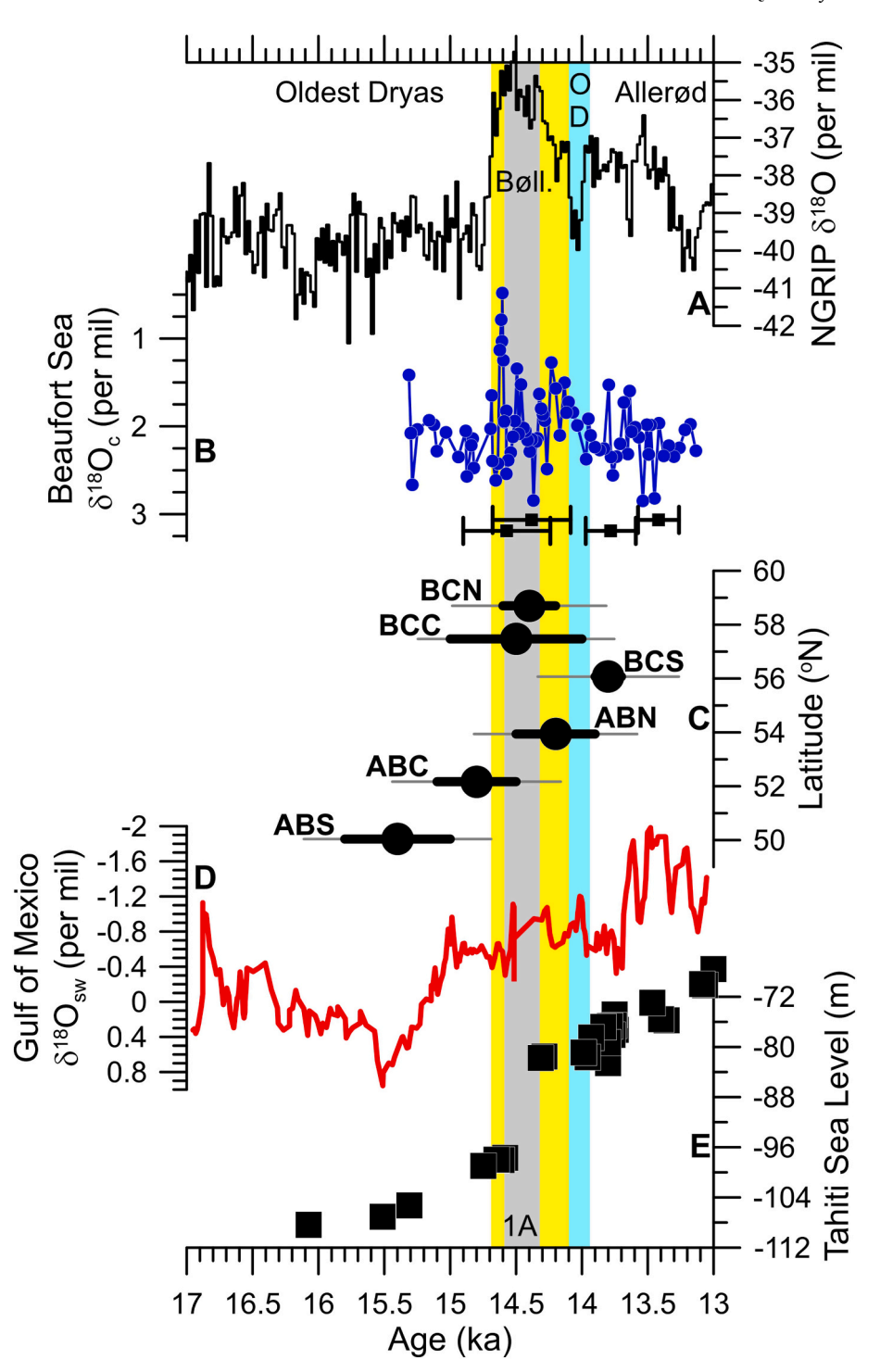


Fig. 5. Atmospheric, oceanic, and ice-sheet records. (A) NGRIP δ^{18} O record with climate periods named (Rasmussen et al., 2006). (B) Planktic δ^{18} O of calcite (c) record from the Beaufort Sea (Fig. 1B); black squares and bars are age-model mean and 2σ uncertainty for 14 C-dated depths (Keigwin et al., 2018). (C) Labeled site 10 Be mean ages and uncertainties; thick horizontal lines are site standard error; thin lines include production-rate uncertainty of $\pm 3.8\%$ (Young et al., 2013). (D) Five-point smoothing of the planktic δ^{18} O of seawater (sw) record from the Gulf of Mexico (Fig. 1B) (Wickert et al., 2013). (E) Tahiti relative sea-level record (Deschamps et al., 2012). Yellow bar is Bølling (Bøll.) that is bisected by the gray bar denoting Meltwater Pulse 1A (1A). Ice-blue bar is Older Dryas (OD). The Oldest Dryas and Allerød are also noted.

timing of deglaciation is hampered by the smaller sample number at the eastern location. Such a true difference in age, with the eastern side of the valley at a similar elevation becoming ice free a millennium after the western side of the valley, would not follow the deglacial pattern reconstructed by Atkinson et al. (2016) where the sites should have similar exposure ages. Following the methodology of Norris et al. (2022) to define a regional deglaciation timing (e.g., they grouped samples from

similar geomorphic settings that were double the distance apart than our ABN sites), we combine them to define a ridge deglaciation at 14.2 ± 0.3 (0.6) ka (n = 11, 1 outlier) (Fig. 5C). Keeping these two sub-sites as separate in our summary does not change our conclusions as the western site still shows the ice sheets had separated by $\sim\!14.3$ ka, which is statistically the same as $\sim\!14.2$ ka. As such, the ABN ages place ice-sheet separation at this portion of the suture zone as occurring before $\sim\!14.2$

ka, with this likely being a close age constraint for the timing of separation.

The ^{10}Be ages at BCS date deglaciation at $13.8\pm0.1~(0.5)~ka~(n=15,$ no outliers) (Figs. 4D and 5C). Given the stratigraphic history of the region, we interpret the deglacial age at BCS to be a close constraint on when the two ice sheets separated. We therefore surmise that the Cordilleran-Laurentide ice sheets had separated at this latitude by $\sim\!13.8~ka$.

One sample at BCC (BCC-2-16, 10.2 ± 0.5 ka) was identified as a young outlier (Fig. 4E), likely undergoing post-depositional movement similar to the outlier at ABN. Despite having then only four samples, BCC still has a consistent ice-free timing with BCS and BCN of 14.5 ± 0.5 (0.7) ka (n = 4, 1 outlier) (Fig. 5C). Because of its location on the Laurentide ice-sheet side of the suture zone, we take the deglacial age of BCC to indicate ice-sheet separation having occurred shortly before \sim 14.5 ka in this region.

BCN is an admixture of boulder and bedrock ages. The four boulders yield a deglacial timing of 14.4 ± 0.2 ka while the six bedrock ages have a deglacial timing of 14.4 ± 0.2 ka. Due to BCN being just to the east of, or on, the ice-sheet suture zone, this deglacial age indicates ice-sheet separation in the north of the suture zone was underway by 14.4 ± 0.2 (0.6) ka (n = 10, no outliers) (Figs. 4F and 5C).

3.2. Timing of cordilleran-laurentide ice-sheet separation

Previous dating constraints on Cordilleran-Laurentide ice-sheet separation, based largely on minimum-limiting radiocarbon and optically stimulated luminescence ages, suggest ice-free conditions before \sim 13.2 ka BP or \sim 16-13 ka, respectively (Froese et al., 2019). Our new $^{10}\mbox{Be}$ ages provide the first direct ages for the spatiotemporal pattern of ice-sheet separation, in turn permitting evaluation of the role of the Cordilleran-Laurentide saddle collapse in rapid sea-level rise. Specifically, ^{10}Be ages from our southernmost site at 50.0°N (ABS) indicate that Cordilleran-Laurentide ice-sheet separation was underway at 15.4 \pm 0.4 ka (Fig. 5C), while ice-sheet separation at 52.2°N (ABC) occurred by 14.8 \pm 0.3 ka (Fig. 5C). Ages from our two northern sites (BCC, 57.5°N; BCN, 58.7°N) date ice-sheet separation occurring by 14.5 \pm 0.5 ka and 14.4 \pm 0.2 ka (Fig. 5C), respectively. Finally, the center of the suture zone between 53.9°N (ABN) and 56.1°N (BCS) deglaciated at 14.2 \pm 0.3 ka and 13.8 \pm 0.1 ka (Fig. 5C), respectively, which places ice-sheet separation occurring shortly before, if not at, these ages.

The deglacial age of 13.8 ± 0.1 ka at site BCS, based on 15^{10} Be exposure ages with no outliers (Fig. 4D), resolves the dating discrepancies in this critical region that was the last part of the Cordilleran-Laurentide saddle to separate according to our suite of 10 Be ages. A radiocarbon age of 14.8 ± 0.4 ka BP on a taiga vole bone near this site (Hebda et al., 2008), previously used to argue for early ice-sheet separation (Potter et al., 2018), is confirmed as an outlier due to contamination by exogenous carbon (Froese et al., 2019). Similarly, nearby lake-sediment records with basal radiocarbon dates of ~ 12.9 ka BP (Pedersen et al., 2016) do not provide accurate controls on the timing of Cordilleran-Laurentide ice-sheet separation in this region as they are only minimum-limiting constraints. Cordilleran-Laurentide separation thus probably began first in the south by 15.4 ± 0.4 ka, then in the north at 58.7° N by 14.4 ± 0.2 ka and progressed to the final zone of ice-sheet confluence at $\sim 56^{\circ}$ N by 13.8 ± 0.1 ka.

This new $^{10}\text{Be-based}$ chronology for Cordilleran-Laurentide ice-sheet separation agrees with the ^{10}Be ages of Stoker et al. (2022) that are from the northwestern margin of the Laurentide ice sheet but to the north of the suture zone (Fig. 1B). Their southernmost site at $\sim\!63.4^\circ\text{N}$ on Cap Mountain has three outliers that date to the LGM: NWT-MM-15-01 (22.5 \pm 0.6 ka), NWT-MM-15-02 (19.8 \pm 0.5 ka), and NWT-MM-15-08 (20.4 \pm 0.6 ka). The next site to the north at $\sim\!65.0^\circ\text{N}$ (Katherine Creek) consists of three samples, with no apparent outliers. The northernmost site at $\sim\!65.2^\circ\text{N}$ (Mackenzie Valley) has four samples with one of these deemed an outlier of LGM age: NW-18-21 (21.2 \pm 0.5 ka).

Consequently, the two higher elevation sites date ice-sheet thinning underway at ${\sim}63.4^{\circ}N$ (Cap Mountain) by 16.8 ± 0.3 ka (0.6) (n = 5, 3 LGM outliers) and at ${\sim}65.0^{\circ}N$ (Katherine Creek) by 17.8 ± 0.2 ka (0.7) (n = 3, 0 outliers). The lowest elevation site at $65.2^{\circ}N$ (Mackenzie Valley) dates northwest Laurentide ice-sheet margin retreat at 14.9 ± 0.7 ka (0.8) (n = 3, 1 LGM outlier), which is consistent with our northernmost site from the Cordilleran-Laurentide suture zone (BCN) that dates separation underway at $58.7^{\circ}N$ by 14.4 ± 0.2 ka.

Similarly, our 10 Be ages from the suture zone are consistent with the 10 Be ages of Dulfer et al. (2021) to the west of the suture zone and Norris et al. (2022) to the east of the suture zone (Fig. 1B). Excluding one LGM outlier that Dulfer et al. (2021) also excluded (RM18-06, 20.6 ± 1.0 ka), the remaining three 10 Be ages date exposure of Mount Spieker at $\sim 55.1^{\circ}$ N from Cordilleran ice-sheet thinning at 15.5 ± 0.8 ka (0.9). We note that our arithmetic mean and uncertainty of 15.5 ± 0.8 ka is very similar to that error-weighted mean reported by Dulfer et al. (2021) of 15.6 ± 0.6 ka. Dulfer et al. (2021) included a snow correction that then allowed their deglacial age to be consistent with other regional deglacial constraints. Our reproduction of this regionally consistent 10 Be age without a snow correction, which Dulfer et al. (2021) noted as highly uncertain, supports our methodology.

Mount Spieker is ~100 km south-southeast of our site BCS, making it the closest site for comparison (ABN is ~200 km southeast of Mount Spieker). Dulfer et al. (2021) show that Cordilleran ice-sheet thinning had commenced by 15.5 \pm 0.8 ka, exposing Mt. Spieker as a nunatak. We then demonstrate ice-sheet thinning to have culminated in Cordilleran-Laurentide ice-sheet separation by 13.8 \pm 0.1 ka at BCS. We note that our ABN site, while twice as far away from Mount Spieker, has a similar modern-day elevation as Mount Spieker vet became ice free 14.2 ± 0.3 ka. This difference in timing could reflect the limited number (n = 3) of Mount Spieker samples relative to ABN, with the former spanning from 16.9 \pm 0.8 ka to 14.2 \pm 0.7 ka (the third age is 15.4 \pm 0.8 ka) while the latter 11 are from 15.6 \pm 0.6 ka to 12.8 \pm 0.3 ka. Alternatively, this difference in timing could reflect a complicated pattern of ice-sheet separation where portions of the suture zone north of ABN became ice-free islands before the two ice sheets fully separated in this region, similar to what Atkinson et al. (2016) reconstructed. This would mean our timing of ice-free conditions at ABN is a closer constraint for complete ice-sheet separation in this region than the Mount Spieker ice-free timing.

The Beaver River site of Norris et al. (2022) deglaciated 14.0 \pm 0.3 ka (0.6) (n = 6, no outliers) based on its error-weighted mean and uncertainty. Using the Laurentide ice-sheet margin retreat pattern Norris et al. (2022) produced, the Beaver River site is up-flow from our ABC site that became ice free at 14.8 \pm 0.3 ka. Our data thus support the Norris et al. (2022) conclusion of rapid southwestern Laurentide ice-sheet margin retreat during the Bølling warm period.

In Fig. 6, we compare our ¹⁰Be ice-sheet separation chronology along with the Dulfer et al. (2021) ¹⁰Be ages to the ice-sheet margin chronology of Dalton et al. (2020). As we are comparing calibrated radiocarbon years to ¹⁰Be years, we use the external uncertainty of the ¹⁰Be mean ages. The 16.8 \pm 1.3 ka BP ice margins (Fig. 6A) agree, within uncertainty, with the timing of ice-free conditions at ABS at 15.4 \pm 0.7 ka, but not ABC at 14.8 \pm 0.6 ka. This would suggest that the ice margins separated slower between ABS and ABC than in Dalton et al. (2020). The 16.1 ± 1.4 ka BP ice margins through 13.5 ± 1.5 ka BP ice margins (Fig. 6B–F) agree with ABC at 14.8 \pm 0.6 ka and ABN at 14.2 \pm 0.6 ka due to the large uncertainties on the Dalton et al. (2020) calibrated margins. This is also the case for Mount Spieker's ice-free timing at 15.5 \pm 0.9 ka. Dalton et al. (2020) places Cordilleran-Laurentide separation as complete in our study region at 14.9 \pm 1.3 ka BP, which agrees with the ice-free timing at BCS (13.8 \pm 0.5 ka), BCC (14.5 \pm 0.7 ka), and BCN $(14.4 \pm 0.6 \text{ ka})$. As such, we find that the ¹⁰Be chronology for Cordilleran-Laurentide ice-sheet separation is consistent, within chronological uncertainties, with that of Dalton et al. (2020). However, when only considering the ¹⁰Be ages, our results suggest that BCS

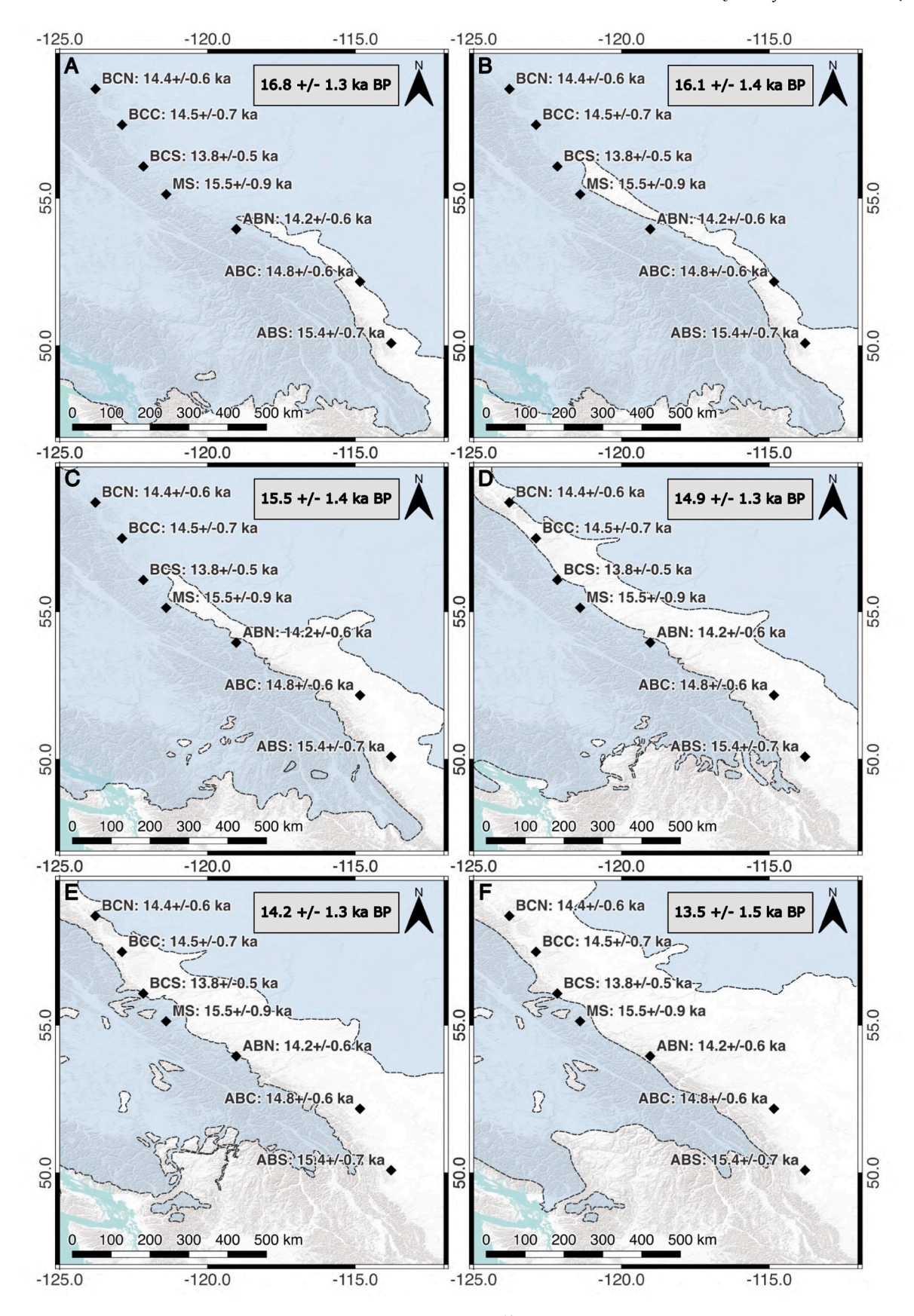


Fig. 6. Ice-margin comparison. Comparison of the ABS to BCN and Mount Spieker (MS) 10 Be mean ages with external uncertainty to the ice-margin maps of Dalton et al. (2020) in calibrated kilo annum with 1σ uncertainty. (A) 14.0^{-14} C ka. (B) 13.5^{-14} C ka. (C) 13.0^{-14} C ka. (D) 12.5^{-14} C ka. (E) 12.0^{-14} C ka. (F) 11.5^{-14} C ka.

deglaciated after BCN (Fig. 1A), noting the above discussed different geomorphic settings of each site relative to constraints on the location of final ice-sheet separation. This would mean that the northern portion of the suture zone separated farther southwards in a similar manner to the northward-progressing separation of the southern portion of the suture zone.

Oceanic records of meltwater discharge support our new ¹⁰Be chronology of ice-sheet separation. In the Gulf of Mexico (Fig. 1B) where the southern half of the saddle-collapse meltwater was discharged (Clark et al., 2001; Tarasov and Peltier, 2005; Wickert et al., 2013; Wickert, 2016), planktic foraminiferal oxygen isotope ratios corrected for temperature began to decrease at ~15.5 ka BP (Fig. 5D) (Wickert et al., 2013), consistent with meltwater discharge from southern ice-sheet separation commencing by ~15.4 ka (Fig. 5C). Sediment provenance indicates that a significant fraction of this meltwater was sourced from the western Laurentide saddle-collapse region (Monterro-Serrano et al., 2009). In the Beaufort Sea off the Mackenzie River (Fig. 1B) where the northern part of the saddle collapse drained (Clark et al., 2001; Tarasov and Peltier, 2005; Wickert, 2016), planktic foraminiferal oxygen isotope ratios decreased at \sim 14.6 ka BP and subsequently increased by 14.6 \pm 0.3 ka BP (Fig. 5B) (Keigwin et al., 2018). Though interpretation of the Beaufort Sea record is subject to radiocarbon reservoir-correction

uncertainties (Keigwin et al., 2018), the temporal trend in Beaufort Sea oxygen isotope composition is consistent with our 10 Be ages from the northern suture-zone, which show that most of the ice-sheet separation had finished by ~ 14.4 ka (Fig. 5C).

Based on the ¹⁰Be chronology presented here, the separation of the Cordilleran-Laurentide ice sheets spanned at least ~1100 years to ~2100 years. Our ¹⁰Be ages date Cordilleran-Laurentide ice-sheet separation in the southernmost sector beginning by ~15.4 ka during the Oldest Dryas (Fig. 5A–C), meaning that the saddle collapse commenced before this time. Cordilleran-Laurentide saddle collapse was not likely triggered by the Bølling warming at ~14.7 ka (Fig. 5A). Rather, the saddle collapse and subsequent ice-sheet separation continued through the Bølling, concluding by ~13.8 ka at the end of the Bølling to during the Older Dryas to Allerød, given production-rate uncertainties (Fig. 5A) (Rasmussen et al., 2006; Clark et al., 2012). However, the ¹⁰Be ages suggest that the Bølling warming could have increased the rate of saddle collapse and attendant sea-level rise contribution. Five-out-of-six ¹⁰Be sites overlap with the Bølling warm period when production-rate uncertainties are considered (Fig. 5A–C).

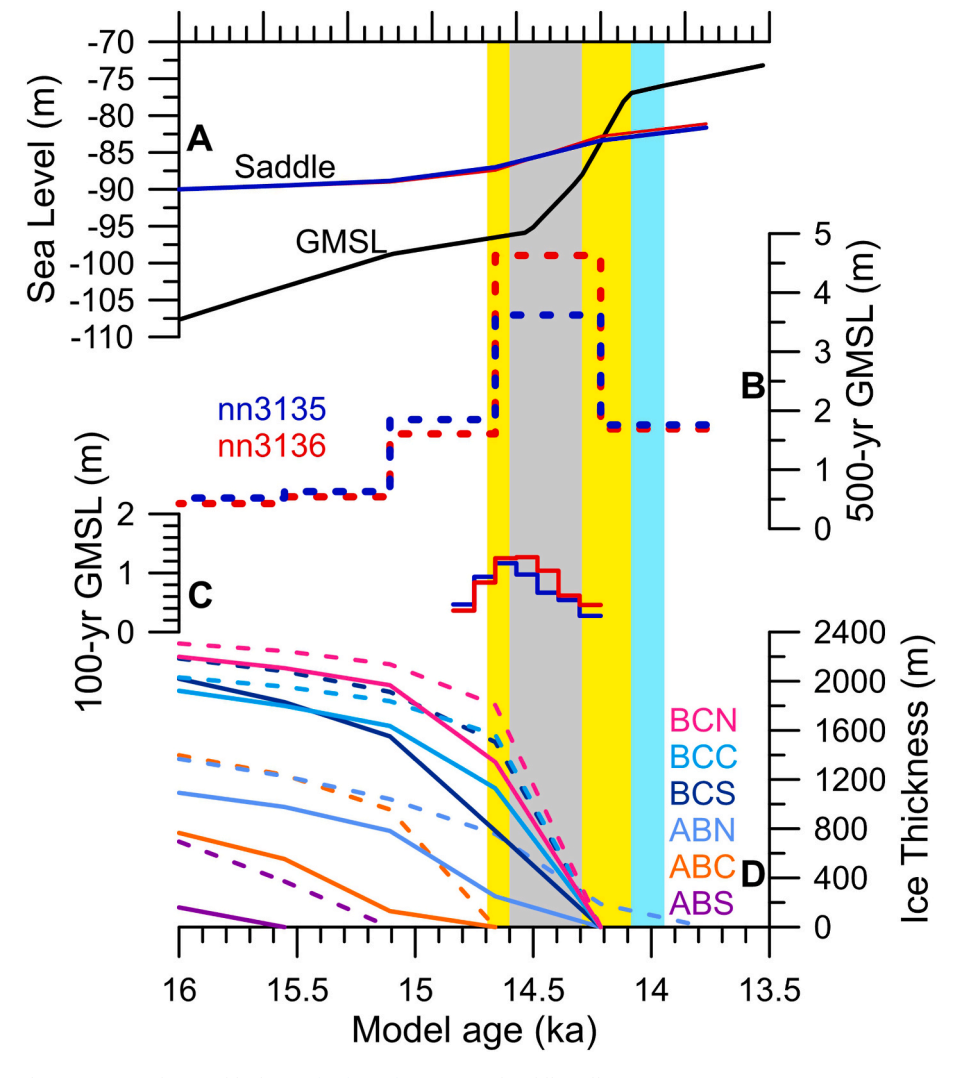


Fig. 7. Ice-sheet model results. (A) GMSL change (black; Lambeck et al., 2014) and saddle collapse region (50–65°N, 105–125°W) contributions to GMSL (blue = nn3135; red = nn3136), which are arbitrarily graphed as starting at -90 m at 16 ka. (B) Saddle collapse GMSL contribution in 500-year increments (blue = nn3135; red = nn3136). (C) Same as (B) but at 100-year increments for the period 14.7-14.0 ka. (D) Ice thickness at our six sites for nn3135 (solid) and nn3136 (dashed). Yellow bar is the Bølling that is bisected by the gray bar denoting Meltwater Pulse 1A; ice-blue bar is the Older Dryas.

3.3. Sea-level rise from saddle collapse

We estimate Cordilleran-Laurentide saddle-collapse contributions to GMSL rise and MWP-1A with the two ice-sheet model simulations (termed nn3135 and nn3136) whose retreat histories are consistent with the new ^{10}Be ages. In these models, the thinning of the saddle began by 16.0–15.5 ka and ends by 14.0–13.5 ka (Fig. 7D). Ice-sheet mass loss in the saddle-collapse zone (Fig. 1B) contributed 6.2–7.2 m to GMSL rise in the 15.5-14.0 ka period (Fig. 7A and B). Across this interval, GMSL rose 19–20 m (Fig. 7A) (Clark et al., 2009; Lambeck et al., 2014), meaning the saddle collapse contributed $\sim\!1/3$ of the GMSL rise that occurred from $\sim\!15.5$ ka to $\sim\!14.0$ ka.

In the Bølling time window that encompasses MWP-1A, the two icesheet models simulate a peak 300-year saddle-collapse contribution of 3.1 m (nn3135) and 3.6 m (nn3136) to GMSL rise (Fig. 7C), which supports the hypothesis that Bølling warming increased the rate of saddle collapse. While based on only two ice-sheet model runs and not a larger ensemble (e.g., Tarasov et al., 2012), the simulated 3.1-3.6 m range of saddle-collapse contribution to MWP-1A is consistent with the lower end of the 3-6 m range simulated by Gregoire et al. (2016) and the ~3.4 m of Stoker et al. (2022). Our total GMSL contribution from the saddle collapse of 6.2–7.2 m is slightly larger than the \sim 6 m upper end of Gregoire et al. (2016). However, the new ¹⁰Be ages show that ice-sheet separation, and by extension the saddle collapse, occurred over at least 1 to 2 millennia. This largely rules out greater saddle-collapse contributions to MWP-1A, which could have potentially happened if the collapse occurred over a few centuries (Gregoire et al., 2012; Gregoire et al., 2016 Lambeck et al., 2017; Lin et al., 2021).

GMSL during MWP-1A rose by at least ~ 9 m and up to ~ 16 m (Liu et al., 2016). Our combined 10 Be ages and ice-sheet models suggest that the Cordilleran-Laurentide saddle collapse contributed $\sim 20-40\%$ of the meltwater to MWP-1A. Another study estimated MWP-1A's magnitude at 16–20 m GMSL rise (Lin et al., 2021), which would reduce the saddle-collapse contribution to only $\sim 15-25\%$. However, this greater MWP-1A magnitude also assumes a much larger saddle-collapse contribution to MWP-1A (Lambeck et al., 2017; Lin et al., 2021) than we reconstruct, suggesting their total magnitude of MWP-1A is overestimated.

These estimated MWP-1A contributions are only for the saddle-collapse region; other sectors of the Cordilleran and Laurentide ice sheets would have contributed to the MWP (e.g., Tarasov et al., 2012; Barth et al., 2019; Norris et al., 2022) along with other ice sheets, such as the Fennoscandian, Barents-Kara and Antarctic ice sheets (e.g., Carlson and Clark, 2012; Weber et al., 2014; Brendryen et al., 2020; Lin et al., 2021). Consequently, MWP-1A reflects a coincidental period of rapid ice-sheet mass loss from at least several ice sheets and not an isolated causal instability in any one ice sheet.

4. Summary

Our 10 Be chronology from the suture zone of the Cordilleran and Laurentide ice sheets dates the separation of these two ice sheets as underway by ~ 15.4 ka with completion by ~ 13.8 ka. The collapse of the saddle connecting these two ice sheets thus occurred over at least one to two millennia, which raised GMSL by 6.2–7.2 m. This saddle collapse overlapped with MWP-1A and contributed 3.1–3.6 m to this MWP, which is a smaller contribution than recent estimates.

Declaration of competing interest

The authors declare that they have no known competing financial interests or personal relationships that could have appeared to influence the work reported in this paper.

Data availability

All data presented in this paper are available in the Tables S1, S2, and S3.

Acknowledgements

H. Bervid assisted with sample collection in the field. J. Bednarski, T. Ferbey, G. Hartman, A. Hickin, and D. Utting provided insight into erratic locations. Reviews by J. Licciardi and B. Stoker with M. Margold improved this manuscript. This research was supported by U.S. National Science Foundation (EAR-1552230; AEC, JC, ECBC), Natural Sciences and Engineering Research Council of Canada Discovery Grants (AVR, GAM, LT), and Australian Nuclear Science Technology Organisation Research Portal Proposal AP12612 (DHR).

Appendix A. Supplementary data

Supplementary data to this article can be found online at https://doi.org/10.1016/j.quascirev.2024.108554.

References

- Atkinson, N., Pawley, S., Utting, D.J., 2016. Flow-pattern evolution of the Laurentide and Cordilleran ice sheets across west-central Alberta, Canada: implications for ice sheet growth, retreat and dynamics during the last glacial cycle. J. Quat. Sci. 31, 753–768.
- Balco, G., Briner, J., Finkel, R.C., Rayburn, J.A., Ridge, J.C., Schaefer, J.M., 2009. Regional beryllium-10 production rate calibration for late-glacial northeastern North America. Quat. Geochronol. 4, 93–107.
- Balco, G., Stone, J.O., Lifton, N.A., Dunai, T.J., 2008. A complete and easily accessible means of calculating surface exposure ages or erosion rates from ¹⁰Be and ²⁶Al measurements. Quat. Geochronol. 3, 174–195.
- Barth, A.M., Marcott, S.A., Licciardi, J.M., Shakun, J.D., 2019. Deglacial thinning of the Laurentide ice sheet in the Adirondack mountains, New York, USA, revealed by ³⁶Cl exposure dating. Paleoceanogr. Paleoclimatol. 34, 2018PA003477.
- Bednarski, J.M., Smith, I.R., 2007. Laurentide and montane glaciation along the Rocky mountain foothills of northeastern British Columbia. Can. J. Earth Sci. 44, 445–457.
- Borchers, B., Marrero, S., Balco, G., Caffee, M., Goehring, B., Lifton, N., Nishiizumi, K., Phillips, F., Schaefer, J., Stone, J., 2016. Geological calibration of spallation production rates in the CRONUS-Earth project. Quat. Geochronol. 31, 188–198. https://doi.org/10.1016/j.quageo.2015.01.009.
- Brendryen, J., Haflidason, H., Yokoyama, Y., Haaga, K.A., Hannisdal, B., 2020. Eurasian Ice Sheet collapse was a major source of Meltwater Pulse 1A 14,600 years ago. Nat. Geosci. 13, 363–368.
- Bobrowsky, P., Rutter, N.W., 1992. The Quaternary geologic history of the Canadian Rocky mountains. Géogr. Phys. Quaternaire 46, 5–50.
- Carlson, A.E., 2020. Comment on: deglaciation of the Greenland and Laurentide ice sheets interrupted by glacier advance during abrupt coolings. Quat. Sci. Rev. 240, 106354.
- Carlson, A.E., Clark, P.U., 2012. Ice sheet sources of sea level rise and freshwater discharge during the last deglaciation. Rev. Geophys. 50, 2011RG000371.
- Carlson, A.E., Anslow, F.S., Obbink, E.A., LeGrande, A.N., Ullman, D.J., Licciardi, J.M., 2009. Surface-melt driven Laurentide ice sheet retreat during the early Holocene. Geophys. Res. Lett. 36, L24502.
- Catto, N., Liverman, D.G.E., Bobrowsky, P.T., Rutter, N., 1996. Laurentide, cordilleran, and montane glaciation in the western Peace river Grande prairie region, Alberta and British Columbia, Canada. Quat. Int. 32, 21–32.
- Clark, J., Carlson, A.E., Reyes, A.V., Carlson, E.C.B., Guillaume, L., Milne, G.A., Tarasov, L., Caffee, M., Wilcken, K., Rood, D.H., 2022. The age of the opening of the Ice-Free Corridor and implications for the peopling of the America. Proc. Natl. Acad. Sci. USA 119, e2118558119.
- Clark, P.U., Dyke, A.S., Shakun, J.D., Carlson, A.E., Clark, J., Wohlfarth, B., Mitrovica, J. X., Hostetler, S.W., McCabe, A.M., 2009. The last glacial maximum. Science 325, 710–714.
- Clark, P.U., Shakun, J.D., Baker, P.A., Bartlein, P.J., Brewer, S., Brook, E.J., Carlson, A.E., Cheng, H., Kaufman, D.S., Liu, Z., Marchitto, T.M., Mix, A.C., Morrill, C., Otto-Bliesner, B., Pahnke, K., Russell, J.M., Whitlock, C., Adkins, J.F., Blois, J.L., Clark, J., Colman, S.C., Curry, W.B., Flower, B.P., He, F., Johnson, T.C., Lynch-Stieglitz, J., Markgraf, V., McManus, J.F., Mitrovica, J.X., Moreno, P.I., Williams, J.W., 2012. Global climate evolution during the last deglaciation. Proc. Natl. Acad. Sci. USA 109, E1134–E1142. 2012.
- Clark, P.U., Marshall, S.J., Clarke, G.K.C., Hostetler, S.W., Licciardi, J.M., Teller, J.T., 2001. Freshwater forcing of abrupt climate change during the last glaciation. Science 293, 283–287.
- Corbett, L.B., Bierman, P.R., Rood, D.H., 2016. Constraining multi-stage exposure-burial scenarios for boulders preserved beneath cold-based glacial ice in Thule, northwest Greenland. Earth Planet Sci. Lett. 440, 147–157.
- Cuzzone, J.K., Clark, P.U., Carlson, A.E., Ullman, D.J., Rinterknecht, V.R., Milne, G.A., Pekka, J., Wohlfarth, B., Marcott, S.A., Caffee, M., 2016. Final deglaciation of the

- Scandinavian Ice Sheet and implications for the Holocene global sea-level budget. Earth Planet Sci. Lett. 448, 34–41.
- Dalton, A.S., Margold, M., Stokes, C.R., Tarasov, L., Dyke, A.S., Adams, R.S., Allard, S., Arends, H.E., Atkinson, N., Attig, J.W., Barnett, P.J., 2020. An updated ice margin chronology for the North American Ice Sheet Complex. Quat. Sci. Rev. 234, 106223.
- Deschamps, P., Durand, N., Bard, E., Hamelin, B., Camoin, G., Thomas, A.L., Henderson, G.M., Okuno, J., Yokoyama, Y., 2012. Ice-sheet collapse and sea-level rise at the Bølling warming 14,600 years ago. Nature 483, 559–564.
- Dulfer, H.E., Margold, M., Engel, Z., Braucher, R., Aster Team, 2021. Using ¹⁰Be dating to determine when the cordilleran ice sheet stopped flowing over the Canadian Rocky mountains. Quat. Res. 102, 222–233.
- Dyke, A.S., 2004. An outline of North American deglaciation with emphasis on central and northern Canada. Dev. Quat. Sci. 2, 373–424.
- Farrell, W.E., Clark, J.A., 1976. On postglacial sea level. Geophys. J. Roy. Astron. Soc. 46, 647–667
- Froese, D., Young, J.M., Norris, S.L., Margold, M., 2019. Availability and viability of the ice-free corridor and Pacific coast routes for the peopling of the America. SAA Archaeol. Rec. 19, 27–33.
- Gomez, N., Gregoire, L.J., Mitrovica, J.X., Payne, A.J., 2015. Laurentide-Cordilleran Ice Sheet saddle collapse as a contribution to meltwater pulse 1A. Geophys. Res. Lett. 42, 3954–3962.
- Gregoire, L.J., Otto-Bliesner, B., Valdes, P.J., Ivanovic, R., 2016. Abrupt Bølling warming and ice saddle collapse contributions to the Meltwater Pulse 1a rapid sea level rise. Geophys. Res. Lett. 43, 9130–9137.
- Gregoire, L.J., Payne, A.J., Valdes, P.J., 2012. Deglacial rapid sea level rises caused by ice-sheet saddle collapses. Nature 487, 219–222.
- Hartman, G.M.D., Clague, J.J., 2008. Quaternary stratigraphy and glacial history of the Peace River valley, northeast British Columbia. Can. J. Earth Sci. 45, 549–564.
- Hartman, G.M.D., Clague, J.J., Barendregt, R.W., Reyes, A.V., 2018. Late Wisconsinan Cordilleran and Laurentide glaciation of the Peace River valley east of the Rocky mountains, British Columbia. Can. J. Earth Sci. 55, 1324–1338.
- Hebda, R.J., Burns, J.A., Geertsema, M., Jull, A.J.T., 2008. AMS-dated late Pleistocene taiga vole (Rodentia: *Microtus xanthognathus*) from northeast British Columbia, Canada: a cautionary lesson in chronology. Can. J. Earth Sci. 45, 611–618.
- Hickin, A.S., Lian, O.B., Levson, V.M., 2016. Coalescence of late Wisconsinan Cordilleran and Laurentide ice sheets east of the Rocky mountain foothills in the Dawson Creek region, northeast British Columbia, Canada. Quat. Res. 85, 409–429.
- Huntley, D.H., Hickin, A.S., Lian, O.B., 2016. The pattern and style of deglaciation at the Late Wisconsinan Laurentide and Cordilleran ice sheet limits in northeastern British Columbia. Can. J. Earth Sci. 54, 52–75.
- Jackson, L.E., Phillips, F.M., Shimamura, K., Little, E.S., 1997. Cosmogenic ³⁶Cl dating of the Foothills erratics train, Alberta, Canada. Geology 25, 193–198.
- Keigwin, L.D., Kotsko, S., Zhao, N., Reilly, B., Giosan, L., Driscoll, N.W., 2018. Deglacial floods in the Beaufort Sea preceded Younger Dryas cooling. Nat. Geosci. 11, 599–604.
- Kohl, C., Nishiizumi, K., 1992. Chemical isolation of quartz for measurement of in-situproduced cosmogenic nuclides. Geochem. Cosmochim. Acta 56, 3583–3587.
- Lambeck, K., Rouby, H., Purcell, A., Sun, Y., Sambridge, M., 2014. Sea level and global ice volumes from the last glacial maximum to the Holocene. Proc. Natl. Acad. Sci. USA 111, 15296–15303.
- Lambeck, K., Purcell, A., Zhao, S., 2017. The North American Late Wisconsin ice sheet and mantle viscosity from glacial rebound analyses. Quat. Sci. Rev. 158, 172–210.
- Lemmen, D.S., Duk-Rodkin, A., Bednarski, J.M., 1994. Late glacial drainage systems along the northwestern margin of the Laurentide Ice Sheet. Quat. Sci. Rev. 13, 805–828
- Leydet, D.J., Carlson, A.E., Teller, J.T., Breckenridge, A., Barth, A., Ullman, D.J., Sinclair, G., Milne, G.A., Cuzzone, J.K., Caffee, M., 2018. Eastward routing of glacial Lake Agassiz at the start of the Younger Dryas cold period. Geology 46, 155–158.
- Lifton, N., Sato, T., Dunai, T.J., 2014. Scaling in situ cosmogenic nuclide production rates using analytical approximations to atmospheric cosmic-ray fluxes. Earth Planet Sci. Lett. 386, 149–160.
- Lin, Y., Hibbert, F.D., Whitehouse, P.L., Woodroffe, S.A., Purcell, A., Shennan, I., Bradley, S.L., 2021. A reconciled solution of Meltwater Pulse 1A sources using sealevel fingerprinting. Nature Com 12, 2015.
- Liu, J., Milne, G.A., Kopp, R.E., Clark, P.U., Shennan, I., 2016. Sea-level constraints on the amplitude and source distribution of Meltwater Pulse 1A. Nat. Geosci. 9, 130–134.
- Margold, M., Gosse, J.C., Hidy, A.J., Woywitka, R.J., Young, J.M., Froese, D., 2019. Beryllium-10 dating of the Foothills Erratics Train in Alberta, Canada, indicates detachment of the Laurentide Ice Sheet from the Rocky Mountains at \sim 15 ka. Quat. Res. 92, 1–14.
- Monterro-Serrano, J.C., Bout-Roumazeilles, V., Tribovillard, N., Sionneau, T., Riboulleau, A., Bory, A., Flower, B., 2009. Sedimentary evidence of deglacial megafloods in the northern Gulf of Mexico. Quat. Sci. Rev. 28, 3333–3347.

- Nishiizumi, K., Imamura, M., Caffee, M., Southon, M.W., Finkel, R.C., McAninch, J., 2007. Absolute calibration of ¹⁰Be AMS standards. Nucl. Instrum. Methods B 258, 403–413.
- Norris, S.L., Tarasov, L., Monteath, A.J., Gosse, J.C., Hidy, A.J., Margold, M., Froese, D. G., 2022. Rapid retreat of the southwestern Laurentide ice sheet during the Bølling-Allerød interval. Geology 50, 417–421.
- Pedersen, M.W., Ruter, A., Schweger, C., Friebe, H., Staff, R.A., Kjeldsen, K.K., Mendoza, M.L.Z., Beaudoin, A.B., Zutter, C., Larsen, N.K., Petter, B.A., Nielsen, R., Rainville, R.A., Orlando, L., Meltzer, D.J., Kjær, K.H., Willerslev, E., 2016. Postglacial viability and colonization in North America's ice-free corridor. Nature 537, 45-49.
- Peltier, W.R., 2004. Global glacial isostasy and the surface of the ice-age Earth: the ICE-5G (VM2) model and GRACE. Annu. Rev. Earth Planet Sci. 32, 111–149.
- Peltier, W.R., Drummond, R., 2008. Rheological stratification of the lithosphere: a direct inference based upon the geodetically observed pattern of the glacial isostatic adjustment of the North American continent. Geophys. Res. Lett. 35, L16314.
- Potter, B.A., Baichtal, J.F., Beaudoin, A.B., Fehren-Schmitz, L., Haynes, C.V., Holliday, V. T., Holmes, C.E., Ives, J.W., Kelly, R.L., Llamas, B., Malhi, R.S., Miller, D.S., Reich, D., Reuther, J.D., Schiffels, S., Surovell, T.A., 2018. Current evidence allows multiple models for the peopling of the America. Sci. Adv. 4, eaat5473.
- Rains, R.B., Shaw, J., Sjogren, D.B., Munro-Stasiuk, M.J., Skoye, K.R., Young, R.R., Thompson, R.T., 2002. Subglacial tunnel channels, Porcupine Hills, southwest Alberta, Canada. Quat. Int. 90, 57–65.
- Rasmussen, S.O., Andersen, K.K., Svensson, A.M., Steffensen, J.P., Vinther, B.M., Clausen, H.B., Siggaard-Andersen, M.-L., Johnsen, S.J., Larsen, L.B., Dahl-Jensen, D., Bigler, M., Röthlisberger, R., Fischer, H., Goto-Azuma, K., Hansson, M.E., Ruth, U., 2006. A new Greenland ice core chronology for the last glacial termination. J. Geophys. Res. 111, D06102.
- Reyes, A.V., Carlson, A.E., Milne, G.A., Tarasov, L., Riming, J.R., Caffee, M.W., 2022. Revised chronology of northwest Laurentide ice-sheet deglaciation from ¹⁰Be exposure ages on boulder erratics. Quat. Sci. Rev. 277, 107369.
- Sharma, P., Bourgeois, M., Elmore, D., Granger, D., Lipschutz, M.E., Ma, X., Miller, T., Mueller, K., Rickey, F., Simms, P., Vogt, S., 2000. PRIME lab AMS performance, upgrades and research applications. Nucl. Instrum. Methods Phys. Res. B 172, 112–123.
- Staiger, J., Gosse, J., Toracinta, R., Oglesby, B., Fastook, J., Johnson, J.V., 2007. Atmospheric scaling of cosmogenic nuclide production: climate effect. J. Geophys. Res. 112, B02205.
- Stalker, A.M., 1956. The erratics train, foothills of Alberta. Geol. Surv. Can. Bull. 37, 32.
 Stoker, B.J., Margold, M., Gosse, J.C., Hidy, A.J., Monteath, A.J., Young, J.M., Gandy, N., Gregoire, L.J., Norris, S.L., Froese, D., 2022. The collapse of the Cordilleran-Laurentide ice saddle and early opening of the Mackenzie Valley, Northwest Territories, Canada, constrained by ¹⁰Be exposure dating. Cryosphere 16, 4865–4886.
- Tarasov, L., Peltier, W.R., 2005. Arctic freshwater forcing of the Younger Dryas cold reversal. Nature 435, 662–665.
- Tarasov, L., Dyke, A.S., Neal, R.M., Peltier, W.R., 2012. A data-calibrated distribution of deglacial chronologies for the North American ice complex from glaciological modeling. Earth Planet Sci. Lett. 315–316, 30–40.
- Ullman, D.J., Carlson, A.E., Hostetler, S.W., Clark, P.U., Cuzzone, J., Milne, G.A., Winsor, K., Caffee, M., 2016. Final Laurentide ice-sheet deglaciation and Holocene climate-sea level change. Quat. Sci. Rev. 152, 49–59.
- Utting, D.J., Atkinson, N., 2019. Proglacial lakes and the retreat pattern of the southwest Laurentide ice sheet across Alberta, Canada. Quat. Sci. Rev. 225, 106034.
- Utting, D.J., Atkinson, N., Pawley, S., Livingstone, S.J., 2016. Reconstructing the confluence zone between Laurentide and Cordilleran ice sheets along the Rocky Mountains foothills, south-west Alberta. J. Quat. Sci. 31, 769–787.
- Weber, M.E., Clark, P.U., Kuhn, G., Timmermann, A., Sprenk, D., Gladstone, R., Zhang, X., Lohmann, G., Menviel, L., Chikamoto, M.O., Friedrich, T., Ohlwein, C., 2014. Millennial-scale variability in Antarctic ice-sheet discharge during the last deglaciation. Nature 510, 134–138.
- Wickert, A.D., 2016. Reconstruction of North American drainage basins and river discharge since the last glacial maximum. Earth Surf. Dyn. 4, 831–869.
- Wickert, A.D., Mitrovica, J.X., Williams, C., Anderson, R.S., 2013. Gradual demise of a thin southern Laurentide ice sheet recorded by Mississippi drainage. Nature 502, 668–671.
- Wilcken, K.M., Fink, D., Hotchkis, M., Garton, D., Button, D., Mann, M., Kitchen, R., Hauser, T., O'Connor, A., 2017. Accelerator mass spectrometry on SIRIUS: new 6MV spectrometer at ANSTO. Nucl. Instrum. Methods B 406, 278–282.
- Young, N.E., Briner, J.P., Schaefer, J.M., Miller, G.H., Lesnek, A.J., Crump, S.E., Thomas, E.K., Pendleton, S.L., Cuzzone, J., Lamp, J., Zimmerman, S., Caffee, M., 2020. Reply to Carlson (2020) comment on "Deglaciation of the Greenland and Laurentide ice sheets interrupted by glacier advance during abrupt coolings". Quat. Sci. Rev. 240, 106329.
- Young, N.E., Schaefer, J.M., Briner, J.P., Goehring, B.M., 2013. A Be-10 production- rate calibration for the Arctic. J. Quat. Sci. 28, 515–526.